Journal of Sea Research 205 (2025) 102594

Contents lists available at ScienceDirect

Journal of Sea Research

journal homepage: www.elsevier.com/locate/seares

Accelerated land loss and nuisance flooding potential in the Barataria Basin: The impacts of land subsidence, sea-level rise, and tidal dynamics

Byungho Kang [1,*], Surui Xie

Department of Civil and Environmental Engineering, University of Houston, Houston, TX 77204, USA

ARTICLE INFO

Keywords:
Inundation
Tides
Land subsidence
Sea level rise
Sedimentation

ABSTRACT

The Barataria Basin, an ecologically and economically important microtidal interdistributary basin in Louisiana, is experiencing rapid land subsidence and increased coastal inundation.

This study quantifies the combined effects of land subsidence, sea-level rise (SLR), and evolving tidal dynamics within this vulnerable basin. Our analysis reveals a significantly amplifed tides throughout the region, further exacerbating the impacts of subsidence and SLR.

By 2045, the land area predicted to remain above Mean Higher High Water (MHHW) may decrease to approximately 65 % of the area remaining above Mean Sea Level (MSL), indicating that these low-lying regions will likely experience more frequent high-tide inundation events. This escalating flood risk poses a major threat to the Basin's sustainability, emphasizing the importance of integrating tidal dynamics into the adaptive management plans for restoration projects such as the Mid-Barataria Sediment Diversion (MBSD). The research establishes a benchmark for evaluating the relative contributions of different drivers to coastal change and highlights the growing influence of tidal inundation. These findings offer essential insights to guide management strategies in similarly vulnerable coastal regions worldwide.

1. Introduction

Coastal Louisiana's wetlands provide crucial ecological and economic benefits like storm surge protection, diverse species habitats, and support for local industries (CPRA, 2018). Specifically, these areas function as critical habitats, act as natural barriers against storm surges, and enhance water quality via nitrate removal (Cheng et al., 2020; Vaccare et al., 2019). The estimated annual economic contribution of these wetlands reached US$140,000 per hectare in 2011, a value that has likely increased (Costanza et al., 2014). Acting as natural buffers, they also protect critical coastal infrastructure, including facilities that deliver 90 % of the nation's outer continental oil and gas, constituting 20 % of the total national oil and gas supply (Couvillion et al., 2016; CPRA, 2018).

The Barataria Basin stands out as a particularly important wetland ecosystem within Louisiana's Gulf region. According to Nelson et al. (2002), it supports an estimated 97 % of commercially valuable species dependent on the basin and adjacent coastal estuaries. This reliance translates into a substantial contribution to the U.S. commercial seafood harvest, representing 20 % of the national yield or approximately 500 million pounds of fish and shellfish annually. Despite its rich biodiversity and economic significance, however, the Barataria Basin is experiencing alarming rates of land loss. This basin alone contributes to about 25 % of all land loss across the Mississippi Delta Plain (Edmonds et al., 2023), having lost nearly 1100 km^2 of wetland area between 1932 and 2016, roughly 30 % of its original size (Couvillion et al., 2017).

This ongoing land loss stems from a combination of natural and anthropogenic factors. Natural drivers include vertical land motion (influenced by glacial isostatic adjustment, crustal loading, and gravitational compaction), sea-level rise, and reduced fluvial sediment accretion on coastal marshes (Bowman et al., 1995; Inoue et al., 2008; Karegar et al., 2015; Shirzaei et al., 2021). However, recent studies highlight how human interventions, particularly hydrologic alterations and resource extraction, significantly exacerbate these natural processes within the Barataria region (Edmonds et al., 2023). For instance, levees constructed along the Mississippi River to protect urban centers like New Orleans have drastically cut sediment deposition in the basin (Matsushita et al., 2024), leading to accelerated land loss and saltwater

* Corresponding author.
E-mail addresses: byunghokang@kier.re.kr (B. Kang), sxie9@central.uh.edu (S. Xie).
[1] (Present address) Wind energy research department, Korea Institute of Energy Research, Jeju-do, 63357, Republic of Korea

https://doi.org/10.1016/j.seares.2025.102594
Received 11 November 2024; Received in revised form 17 April 2025; Accepted 20 May 2025
Available online 21 May 2025

intrusion. To address the sediment deficit, the *Mid-Barataria Sediment Diversion* (MBSD) project, which aims to redirect sediment-rich river water into the Barataria Basin, received approval from U.S. Army Corps of Engineers (USACE) in 2022 (Törnqvist, 2023). This multibillion-dollar project is expected to reestablish deltaic processes and expand the wetland area over the next few decades, in the hope of reaching a peak increase of 17,300 acres by 2050 (USACE, 2022). However, the project's effectiveness largely depends on its ability to keep pace with future land subsidence rates and sea-level rise (Törnqvist, 2023).

While the MBSD project offers hope for mitigating land loss in the Barataria Basin, the compounding effects of tides, sea-level rise, and land subsidence, remain a critical concern. Globally, high tide flooding (HTF) is escalating. Hsiao et al. (2024) project that future HTF could inundate up to 600 km^2 of southwestern Taiwan, causing substantial economic losses. Along the US Coasts, projections by Thompson et al. (2021) indicate significant increases in minor HTF events by the 2030s. The Barataria Basin is particularly vulnerable to increasing HTF because, in this low-lying region, even the Gulf Coast's relatively small tidal range—when combined with sea-level rise and subsidence—can have a disproportionate flooding impact (Gornitz et al., 1991; Holzer and Bluntzer, 1984; Sweet et al., 2018; Yang et al., 2014). Accurate predictions of coastal inundation, considering the combined effects of sea-level rise, land subsidence, and tidal dynamics, are crucial for hazard mitigation, long-term planning, and evaluating restoration efforts (Mostafiz et al., 2021). Although individual factors like sea-level rise and subsidence have been studied, a detailed analysis of how these factors

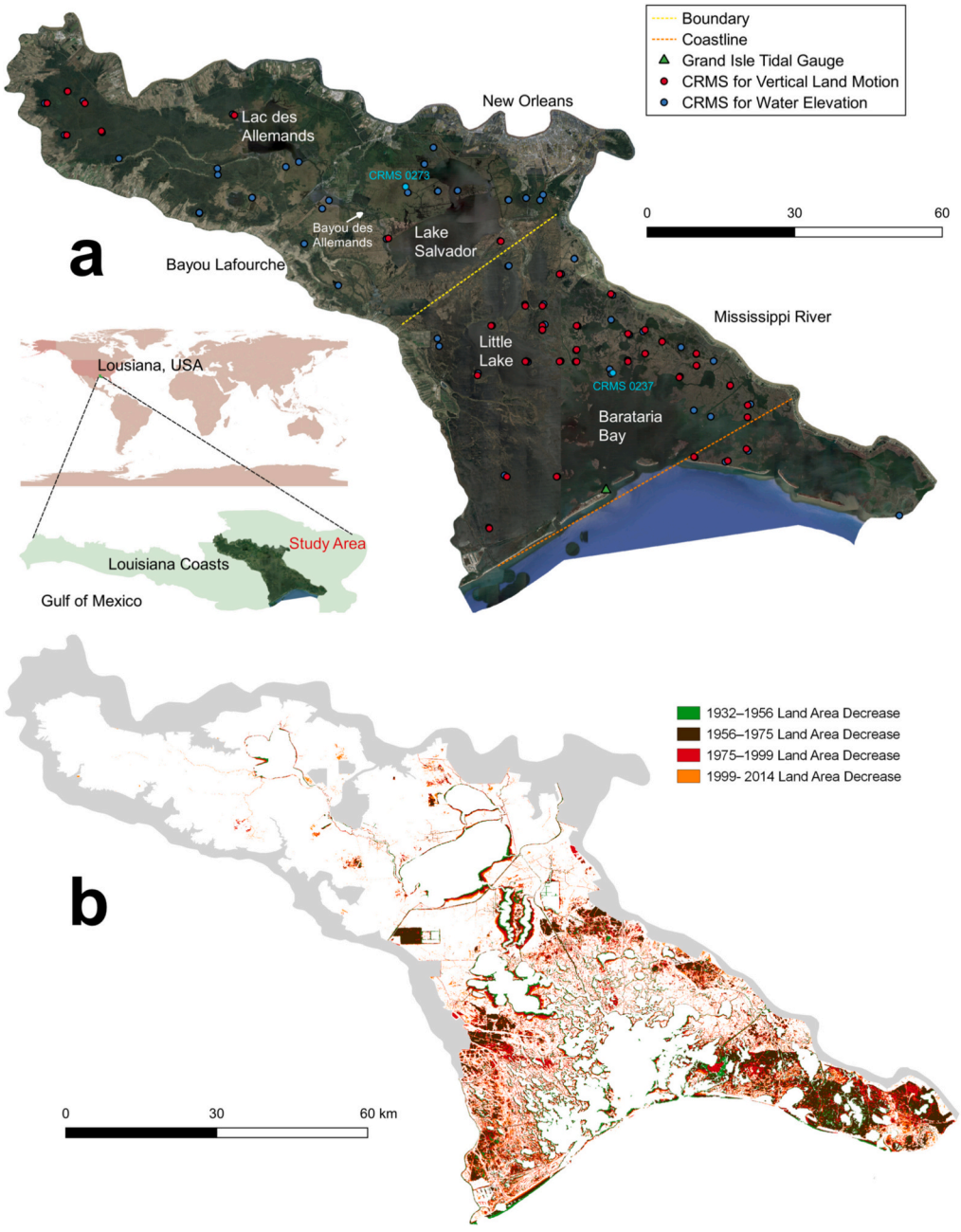

Fig. 1. Study area and historical land loss in the Barataria Basin, Louisiana. (a) Location of the Barataria Basin and the distribution of Coastal Reference Monitoring System (CRMS) stations. The orange dotted line represents the reference coastline used for calculating distances between CRMS stations and the coast, assuming identical tidal characteristics to the Grand Isle tide gauge. (b) Historical land loss from 1932 to 2014 (Couvillion et al., 2017). The gray mask indicates fast land areas (developed or protected zones) excluded from this study (data source: USGS).

interact, particularly with evolving tidal dynamics, to increase coastal vulnerability and inundation risk remains limited.

This study addresses this gap by examining how land subsidence, sea-level rise, and evolving tidal dynamics collectively drive high-tide flood risk in the Barataria Basin. With high-resolution digital elevation model (DEM) and a comprehensive dataset of land subsidence rates, we characterized historical coastal change and predicted several future scenarios. This research provides crucial model benchmarks for understanding future tidal flood risk that are subject to the effects of complex processes, emphasizing the influence of changing tidal dynamics. These benchmarks offer quantitative information for coastal restoration and management strategies.

2. Environmental setting

2.1. Geographical characteristics of the study site

The Mississippi Delta Plain (MDP), a region of considerable economic and ecological value, had a net growth in area over several millennia following the stabilization of sea levels (Day et al., 1997). This growth was caused by various natural factors, such as storm events, river flooding leading to sediment deposition, and the reshaping of distributary channels (avulsions) (Roberts, 1997). However, this trend was interrupted by escalating human activities in the 20th century, resulting in significant wetland loss in coastal Louisiana (Gagliano et al., 1981). Some of these human activities include the construction of levees and the closure of distributaries, which hinder the sediment supply from the Mississippi River to the MDP (Blum and Roberts, 2009), along with alterations in hydrology caused by canal construction (Day et al., 2000).

Within the MDP, the Barataria Basin (Fig. 1) serves as a typical example of the region's susceptibility to land loss due to anthropogenic pressure. The Barataria Basin is a vast interdistributary zone located west of the Mississippi River delta, with a total area of approximately 7100 km^2. The elevation of the basin varies within only 5 m, with high natural levees by the Mississippi River at 4 to 5 m, and marshes near sea level (Byrnes et al., 2019); the average depth of the estuary is about 2 m (Das et al., 2012).

In this study, we focused on the areas excluding the fastlands, where there is dense infrastructure such as levees to protect local human communities and the agricultural lands (the extent is represented by the gray shade in Fig. 1b). Thus, our analysis primarily focuses on a reduced area of 5700 km^2, bordered by the Mississippi River to the east and north, the Bayou Lafourche to the west, and the Gulf of Mexico to the south (Fig. 1a). We divided the study area into two regions based on the intensity of tides: a northwestern wetland habitat featuring freshwater marshes with several large lakes that have minor tides (upper Barataria) and a southeastern zone composed of brackish water and marshes that are connected to the Gulf of Mexico via four tidal passes (lower Barataria) (Das et al., 2012).

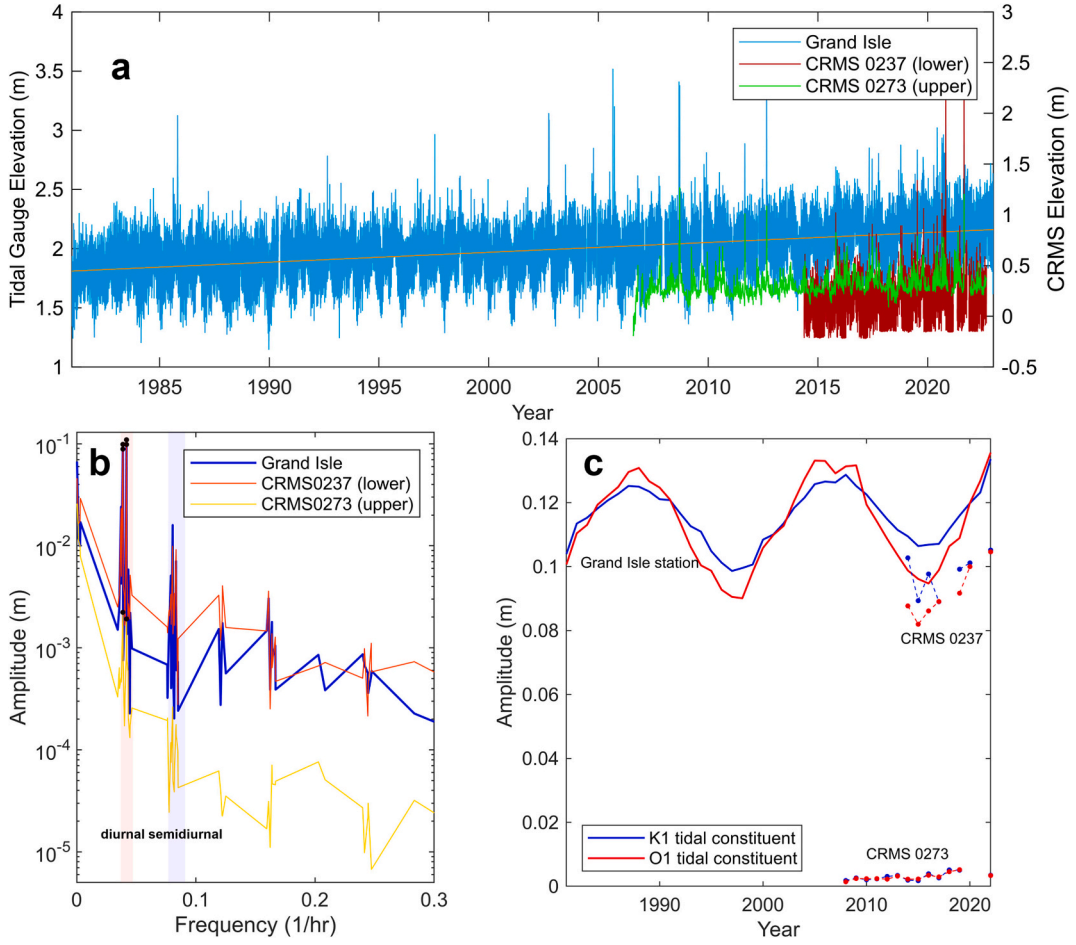

Fig. 2. Tidal characteristics at Grand Isle and CRMS stations in the Barataria Basin. (a) Water level fluctuations at the Grand Isle tide gauge (referenced to station datum) and representative CRMS stations (referenced to NAVD88). Grand Isle measurements reflect both sea-level rise (SLR) and land subsidence, while CRMS data, corrected for instrumental drift, primarily reflect SLR. (b) Tidal spectrum at Grand Isle and representative CRMS stations for 2014, highlighting the dominant diurnal constituents O1 and K1. (c) Yearly amplitudes of O1 and K1 constituents at the Grand Isle tide gauge (1981–2022), illustrating the influence of the 18.6-year nodal cycle.

2.2. Hydrological characteristics and analysis

To accurately characterize the tidal intrusion in the Barataria region, it's important to comprehend the tidal spectrum in the region. We determined the characteristics of ocean tide variations primarily through the data collected by the Grand Isle tidal gauge (29.263 N, 89.957 W; NOAA station ID: 8761724). This gauge was established in 1979, but full records of hourly water elevation were not available until 1981. This study used quality-controlled records from 1981 to 2022 (Fig. 2a). We calculated a relative sea level rise (RSLR) rate of 8.3 mm/yr at this tide gauge, slightly slower than the 9.16 ± 0.37 mm/yr local sea level trend derived from data obtained between 1947 and 2022 by NOAA. The average vertical motion rate of the GPS monument at Grand Isle derived from nearly two decades of continuous measurements is −6.3 ± 0.4 mm/yr (Karegar et al., 2020). These rates are consistent considering different data spans and the vertical rate difference between benchmarks anchored at different depths (e.g., the near-surface Holocene sediment compaction rate is a function of foundation depth). Nevertheless, in this study, we adopted a geocentric sea-level rise rate of 3 mm/year for the Gulf of Mexico. The rate represents a slight increase from the 2.9 ± 0.4 mm/year determined by satellite altimetry data from 1992 to 2014, as it accounts for recent accelerations in sea-level rise (Pahl, 2017).

After detrending the water elevation time series based on the RLSR rate, we analyzed the major tide constituents yearly from the Grand Isle water elevation records using T-Tide (Fig. 2b; Pawlowicz et al. (2002)). The F-ratios, calculated as the ratio of amplitudes (K1 + O1) / (M2 + S2), fall between 8 and 13 at Grand Isle, indicating a strong dominance of the diurnal tidal constituents over the semi-diurnal constituents. Further, comparison of tidal analyses using data from two illustrative Coastal Reference Monitoring System (CRMS)—alongside Grand Isle measurements demonstrate that, within the diurnal tidal spectrum, the O1 and K1 constituents dominate in both regions. In addition, we applied T-Tide to the detrended time series depicted in Fig. 2a to evaluate the temporal variations in the amplitude of diurnal tide constituents at Grand Isle. Notably, the results reveal the influence of the 18.6-year lunar nodal cycle (Fig. 2c).

3. Material and methods

3.1. Water level and land elevation data

To analyze local water level changes, we used continuous water level data collected between 2007 and 2022 from all 91 available CRMS stations within the Barataria Basin (Fig. 1a). The timeframe of 2007–2022 corresponds to the operational period of most CRMS stations in the basin, ensuring a consistent and comprehensive dataset. These stations represent a subset of the larger CRMS network, which includes approximately 391 sites across coastal Louisiana and a total of around 550 stations.

This subset comprised 49 CRMS stations near inlets (lower Barataria) and 42 CRMS stations situated further from the sea (upper Barataria). For each CRMS station, the distance to the coastline was determined using the shortest cross-track distance to a reference line, shown as orange dotted lines in Fig. 1a.

As part of data quality assurance, the water elevation records were corrected to mitigate issues related to biofouling and instrument drift, and erroneous data points were removed by the data provider (CPRA, 2022). Also, the raw water levels were recorded in orthometric heights, with the geoid model transitioning from GEOID99 to GEOID12A on September 30th, 2013. To align the measurements with a consistent height datum for each CRMS location (using GEOID12A), we applied a small correction specific to each CRMS location.

We used data from a subset of 40 CRMS stations equipped with surface-elevation table–marker horizon (RSET-MH) instruments within Barataria basin to estimate the land subsidence rate. These instruments provide one of the most direct measures of near-surface processes, capturing changes from organic matter decomposition, sediment compaction, and vertical accretion, as well as deeper subsidence due to glacial isostatic adjustment, tectonics, or fluid withdrawal (Jankowski et al., 2017). While some RSET rods lack sleeves or stable anchors and may not fully distinguish shallow compaction from deeper subsidence (Byrnes et al., 2019), this dataset remains the most comprehensive for quantifying relative surface elevation changes across coastal Louisiana.

To estimate the change in land area, we utilized a Digital Elevation Model (DEM) derived from the Coastal National Elevation Database (CoNED) topobathymetric digital elevation models (TBDEMs: see Fig. 3a). This comprehensive model integrates both topographical (land elevation) and bathymetric (water depth) representations, providing the highest resolution elevation model for the region among public-available DEMs. The vertical datum used for the DEM was North American Vertical Datum 1988 (NAVD88), with a geoid model of GEOID12B. There were no significant disparities between the use of GEIOD12A and GEOID12B for this study. While the original spatial resolution of the CoNED TBDEMs was 3 m, we downsampled it to 5 m to reduce the computational load of our analyses.

3.2. Sea level and high-water measurement and prediction

To simplify the notation within our study, we define the Mean Sea Level (MSL) for a given year as the average water elevation during that year. Similarly, we define the Mean Higher High Water (MHHW) of a year as the average of daily maximums throughout the year (note that MHHW traditionally refers to the higher high water average over an 18.6-year period). We estimated both the MSL and MHHW for each observational year from 2007 to 2022 at every CRMS station across the Barataria region.

To predict future MHHW at each CRMS station, we used a method that accounts for tidal constituent variability and the 18.6-year nodal modulation cycle. Directly applying nodal corrections to each CRMS station's O1 and K1 amplitudes was not feasible, as the data duration was not long enough to cover a full nodal cycle. Instead, we leveraged the Grand Isle tidal gauge as a reference station. By comparing yearly tidal amplitudes at each CRMS station to those at Grand Isle, we established an empirical model that uses the amplitude ratio to link tidal heights at Grand Isle and CRMS stations. This approach allowed us to incorporate the nodal cycle and address data gaps without directly extrapolating the modulation for each inland station.

Using T-tide, we firstly estimated the yearly amplitude and phase of the dominant diurnal tide constituents, namely O1 and K1, for each CRMS station throughout 2007 to 2022 (Pawlowicz et al., 2002). We also obtained the amplitudes of the same tidal constituents from the Grand Isle tidal gauge for the corresponding years. We then calculated the amplitude ratio, $R_i(Y)$, between the i-th CRMS station and the reference station for a given year Y:

$$R_i(Y) = \frac{C_i(Y)}{G(Y)} \tag{1}$$

where $C_i(Y)$ represents the amplitudes of O1 and K1 for the i-th CRMS station, and $G(Y)$ refers to the respective values at the Grand Isle tidal gauge. We then predicted future amplitudes at Grand Isle, $\widehat{G}(Y)$, by fitting a sinusoidal model that captures the known 18.6-year tidal modulation (see Fig. 2c). Future tidal amplitudes at each CRMS station were predicted based on the evolving ocean tidal amplitudes ($\widehat{G}(Y)$) and expected amplitude ratio, $\widehat{R}_i(Y)$, which was estimated by accounting for temporal changes between each CRMS station and Grand Isle (as discussed in Section 4.1.2). Multiplying $\widehat{G}(Y)$ by the expected ratio $\widehat{R}_i(Y)$ gives predicted tidal amplitudes at station i:

$$\widehat{C}_i(Y) = \widehat{R}_i(Y) \times \widehat{G}(Y) \tag{2}$$

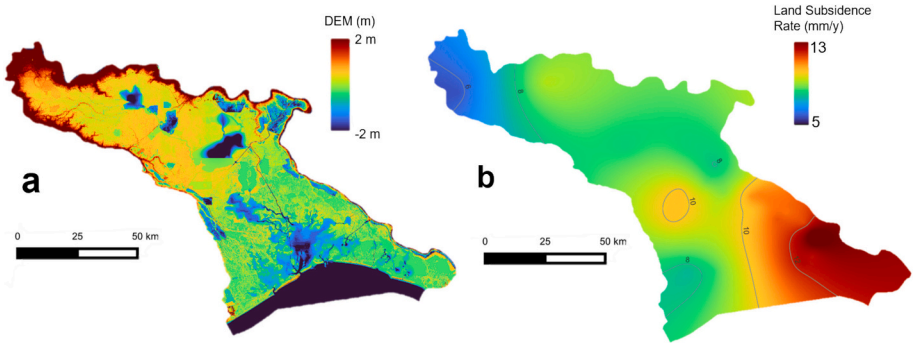

Fig. 3. Digital Elevation Model (DEM) and interpolated land subsidence rates for the Barataria Basin. (a) Topobathymetric DEM for the Barataria Basin (USGS, 2018). (b) Spatial distribution of land subsidence rates.

Note that this model only considers periodic variations in the ocean tidal amplitudes, ignoring secular changes. Next, using the predicted amplitudes and their associated Greenwich phases—both of which have been adjusted for nodal variability—we synthesized a time series of tidal heights for each future year *Y*. From the synthesized time series, we took the daily maximum water levels and average them to obtain yearly mean of tidal highs $\eta_i(Y)$.

Finally, we added a constant eustatic sea-level rise (SLR) rate, $\kappa = 3$ mm/yr (Pahl, 2017), to account for ongoing changes since 2022. Given the MSL at station i in 2022, denoted c_i, the future MHHW was calculated with:

$$\zeta_i(Y) = c_i + \kappa\,(Y - 2022) + \eta_i(Y) \tag{3}$$

By comparing the predicted water levels with land elevations adjusted for land subsidence, we can identify areas most vulnerable to future inundation noting that we did not separately account for accretion processes. The projected MHHW levels serve as an indicator of potential inundation stress on the wetland ecosystem, rather than a definitive measure of permanent land loss. As described in Section 3.4, these predicted water levels were directly used as thresholds to determine which areas will be classified as land or water in future scenarios.

3.3. Interpolation

To estimate the MSL and MHHW for the entire study area the ordinary Kriging method was employed. In the interpolation, we used a linear model, $a + bx$, in which the maximum distance was set to 60 km and lags for semivariance were fixed at 2 km intervals. The selection of these parameters was based on the spatial characteristics observed in the semivariogram. Likewise, the land subsidence rate for the region was also determined using the ordinary Kriging method (Fig. 3b). The linear model was used with the same parameters; lags for semivariance were set at 2 km and the maximum distance was kept at 60 km.

To generate a more realistic interpolation map, we removed several outliers in the land surface elevation change rates. Specifically, we identified and excluded two outlier values, each of which exceeded the mean land subsidence rate for the region by more than three standard deviations. This ensured that our estimates of land subsidence rates across the region were not disproportionately influenced by possible local effects.

3.4. Land area estimation: DEM thresholding

The main objective of this study is to calculate the changes in land area exposed above specific water level thresholds in the Barataria region at different intervals, providing insights into potential inundation. Our methodology involved subtracting or adding the expected cumulative land subsidence from the DEM. Due to limitations in measuring the total subsidence caused by both the deep and shallow processes, different measurement techniques sometimes produce seemingly conflicting results. For example, the land subsidence map from Nienhuis et al. (2017), based on RSET measurements by Jankowski et al. (2017), indicates rates ranging from 6 mm/yr in upper Barataria to 12 mm/yr in lower Barataria. However, Byrnes et al. (2019) report a range of 2 to 7 mm/yr using GPS-derived data. The divergence arises because the GPS-derived land motion rate reflects the vertical motion rate of the monument, which is usually anchored deep into the sediment. In contrast, the RSET-MH method tracks the vertical position of the surface with respect to a rod driven deeply into the sediment, hence the data only reflect the vertical displacement rate of the upper layer. To overcome the discrepancies caused by the inherent limitations of different techniques, we predict the land subsidence based on a range of plausible displacement rates.

We considered cumulative land subsidence based on both the full and a halved land subsidence rate for future land area estimation. This yielded two sets of adjusted land surface heights for above-water land area estimates at different times. In land area estimation, we utilized a 'bathtub' inundation model based on the 'zero-pixel connectivity' and 'four-way pixel connectivity' rules (Poulter and Halpin, 2008; Yunus et al., 2016). Here, 'zero-pixel connectivity' refers to flooding all pixels below the water level threshold (either MSL or MHHW), regardless of their connection to the ocean, and 'four-way pixel connectivity' refers to flooding only the pixels below the threshold and are directly connected to the open water through a path of adjacent pixels. While this simplified approach assumes uniform water levels, neglecting factors such as water surface slopes, tidal currents, and wave action, it is widely used for its practicality and computational efficiency in large-scale coastal inundation assessments (Anderson et al., 2018; Didier et al., 2019; Seenath et al., 2016). Despite its limitations in representing complex hydrodynamic processes, the 'bathtub' method offers a first-order approximation for broad-scale assessment of relative inundation vulnerability, especially when hydrodynamic data or computational resources are limited (Gallien et al., 2011).

In our specific projections for the MSL maps for historic years (1932, 1955, 1975, and 1999), we used the MSL map in 2014 as the reference. Since we do not have observations for the earlier years, we subtracted the cumulative Sea Level Rise (SLR) for each specific year from the 2014 map. The extent of land area was estimated by comparing the resulting MSL map with the adjusted land height (based on either the full or halved land subsidence rate). For the land area prediction of future years 2045 and 2075, we predicted for both MSL and MHHW maps. For the MSL map prediction, we added the expected cumulative SLR to the interpolated 2022 MSL map. On the other hand, as outlined in section 3.2, we predicted the MHHW at each of the CRMS stations and obtained the MHHW maps for the years 2045 and 2075 by interpolation. In both cases, we accounted for cumulative land subsidence by subtracting it from the DEM.

4. Results and discussions

4.1. MHHW prediction

4.1.1. Tidal modulation of amplitude

We analyzed the influence of tidal modulation on the amplitudes of the dominant diurnal constituents (O1 and K1) across 91 CRMS stations in the Barataria Basin from 2007 to 2022. Building upon previous studies, we utilized the T-Tide software to analyze the yearly amplitudes and phases of the tidal constituents O1 and K1 across the study area (Kang and Xie, 2024). Fig. 4 illustrates the temporal variation of the O1 amplitude at these stations. For most coastal CRMS stations, the O1 amplitudes exhibited fluctuations of approximately 3–4 cm per lunar nodal modulation cycle. Similar patterns were observed in the K1 constituent (Fig. A1). While these fluctuations are relatively small, the combined modulation of O1 and K1 amplitudes can significantly influence inundation patterns, particularly in low-relief coastal regions. This influence, however, diminishes with increasing distance from the coast. For instance, the stations that have farthest distances from the coastline exhibit near-zero modulation, indicating limited influence from nodal modulation at these locations. Fig. 5 illustrates the temporal variations in the O1 tidal amplitude observed at coastal CRMS stations. Notably, the amplitude decreased from 13 cm in 2008 to 10 cm in 2014, then increased to 14 cm in 2022 (see Fig. A2 for K1). This pattern suggests a cyclic variation corresponding to the 18.6-year nodal cycle.

Apart from the periodic variation, a relatively small but consistent trend of increase is observed in the tidal amplitudes, particularly at inland stations. As shown in the second row of Fig. 5, the outward shift in amplitude ratio curves (R_i) for O_1 indicates that tides are propagating farther inland with less attenuation, aligning with earlier findings of enhanced tidal intrusion in the region (Kang and Xie, 2024).

The enhanced tides may lead to more frequent and severe flooding in areas previously less affected, highlighting the necessity to study evolving tidal dynamics in coastal and inland waters. This trend in the Barataria Basin mirrors observations in other deltaic systems. For example, the Ganges-Brahmaputra-Meghna Delta has experienced amplified tidal ranges and greater inland propagation due to sea-level rise, land subsidence, and human modifications (Brown and Nicholls, 2015). Similarly, the Yellow Sea Shelf shows altered tidal dynamics driven by both natural and anthropogenic factors (Feng and Feng, 2021). Understanding these changes is vital for effective flood management globally.

4.1.2. Predicting future influence of tidal modulation

We analyzed temporal trends in both baseline (α) and attenuation (β) coefficients for O1 and K1, derived from the exponential relationship between distance (d_i) and amplitude ratio (R_i). In this study, we estimated the baseline coefficient (α) yearly rather than fixing it at a predetermined value, and found no significant temporal trends in α for either tidal constituent (Fig. 6a). The baseline coefficients are typically higher than 1 and bounded by 1.2 for O1 and 1.3 for K1 tide constituents, indicating a larger tidal range of Coastal CRMS station than the Grand Isle tide gauge. Although the baseline coefficients change without a significant trend, Fig. 6b shows a robust trend of decreasing attenuation coefficients (β) over time for both O1 and K1. The yearly attenuation coefficient of O1 decreased by 18 % between 2007 and 2022 (from 0.034 to 0.028), with similar decreases observed for K1 (22 % decrease). The persistent decrease in attenuation (β) cannot be explained solely by the 18.6-year nodal cycle —which causes cyclical increases or decreases in water depth that influence tidal propagation. This decreasing trend spans both the rising and falling phases of the nodal cycle, suggesting that enhanced hydrological connectivity across the region is leading to reduced attenuation independent of nodal modulation (Fig. 4 and Fig. 6b).

To predict future effects of tides, we extrapolated the amplitude ratios based on the observed decreasing trend in attenuation coefficient (β), assuming constant baseline coefficients (α) at their mean observed values. Fig. 6c shows the increase in predicted ratios, $\widehat{R}_i(Y)$. At the 50 km distance to the coastline, the ratios of both tidal constituents are expected to increase from 0.2 in 2022 to around 0.8 in 2075; and the ratios for the inland CRMS stations farthest from coastline will increase to around 0.5 in 2075. These predictions, however, should be interpreted with caution, as the *rate* of β decrease may not be constant. For instance, relatively short (~15-year) observation period may not fully capture longer-term morphological changes that can alter basin hydrodynamics (Allison et al., 2014). Additionally, non-linear feedbacks with sea-level rise could accelerate or reverse the observed trend, while future interventions like the Mid-Barataria Sediment Diversion might shift sediment redistribution and channel configurations. Nonetheless, our approach provides a simplified first-order approximation of future tidal propagation. The predicted increases in amplitude ratios suggest that tides will play a more significant role in the region's hydrodynamics (Fig. 7). The growing influence highlights the need to incorporate evolving tidal dynamics in coastal flood risk assessments, alongside factors like sea-level rise and land subsidence.

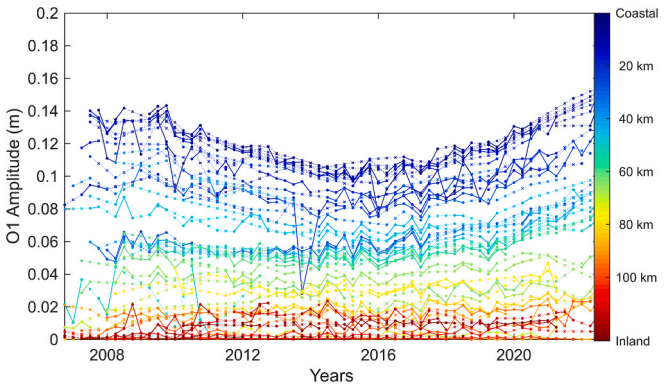

Fig. 4. Tidal amplitude variations. The graph depicts amplitude of O1 tidal constituents, for each quarter from 2007 to 2022 across various CRMS stations, with color grading indicating the relative order of their distances from coastlines. Dots represent observed data; 'x' symbols indicate interpolated values. Stations seaward of the reference coastline are assigned a zero distance.

4.2. Land area projection for past

We estimated the historic land area using the MSL map in comparison to the adjusted DEM vertical height. The land area defined by the DEM above the MSL, measured at 2376 km^2 for zero-connection (Fig. 8a). Also, the default DEM value above 0 m in NAVD 88, without considering the water level or subsidence, measured the land area at 2487 km^2 for zero-connection. Both of these estimates are smaller than the Landsat measurements, which recorded a land area of 2656 km^2 in August 2014. The mismatch between DEM-based land area estimates and Landsat measurements can be partially explained by the local sea level relative to the height datum, and the different characteristics in LiDAR DEM and Landsat optical imagery, as LiDAR can penetrate vegetation and Landsat data reflect the canopy area (García et al., 2018).

While other factors contribute to changes in emergent land area, including permanent conversion to open water, considering sea-level rise (SLR) alone significantly underestimates the observed losses (Fig. 8a). This highlights the need to incorporate land subsidence in understanding the changes in land area relative to sea level. Considering SLR alone substantially underestimates historical land loss, demonstrating the importance of including land subsidence in land loss assessments (Fig. 8a). On the other hand, projections using the full land subsidence rate significantly overestimate the historical land area above MSL. Adjusting the land subsidence rate to half its value improves the

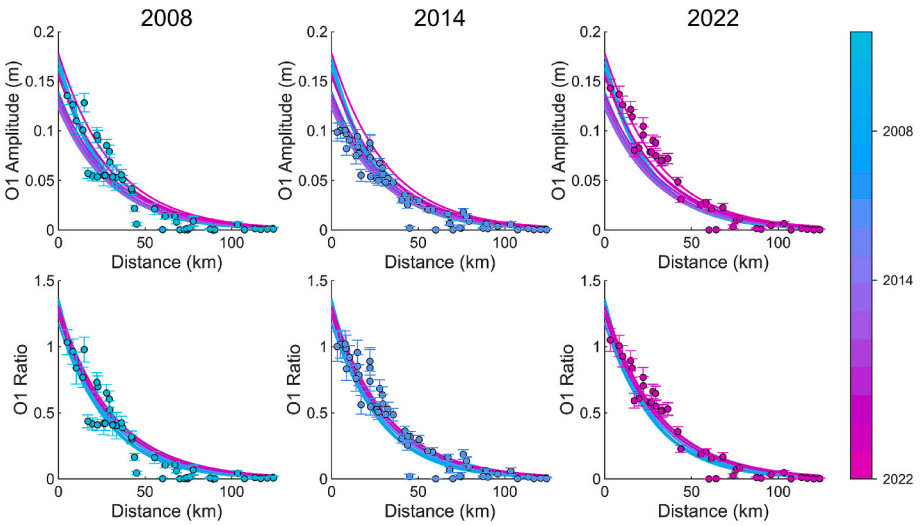

Fig. 5. Top Row: Yearly O1 amplitudes at CRMS stations versus distance from the coastline for the years 2008, 2014, and 2022. Bottom Row: Yearly O1 amplitude ratios (CRMS amplitude/Grand Isle amplitude) versus distance for the same years. In both rows, the exponential decay lines depict the overall attenuation trends based on the entire dataset (2007–2022), modeled using $y = \alpha \times exp(-\beta \times x)$, where '$y$' represents either amplitude or amplitude ratio, x is the distance from the coastline, α is the baseline, and β is the attenuation coefficient. The scatter points in each plot correspond to the specific years 2008, 2014, and 2022. Amplitude errors were estimated using T-Tide, and ratio errors were determined via error propagation.

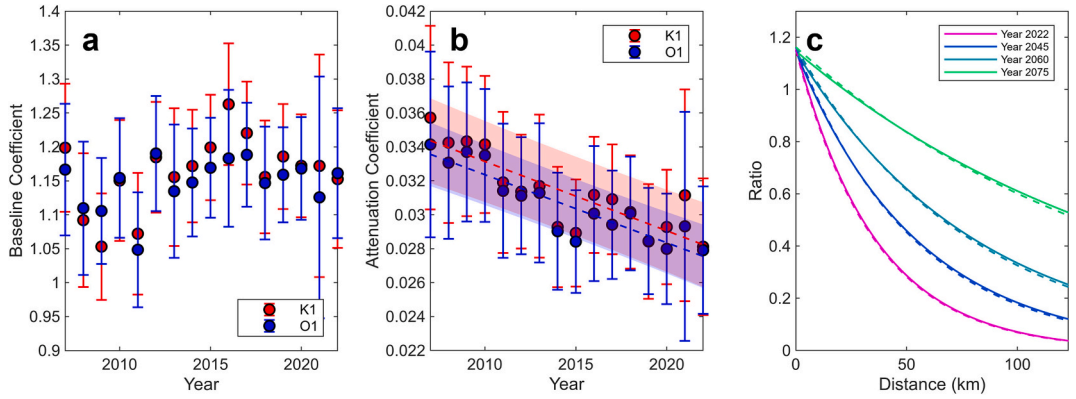

Fig. 6. Trends and future predictions of tidal amplitude ratios. (a) Yearly baseline coefficients (α) for O1 and K1, derived from exponential regression fits of amplitude ratios versus distance. Linear regression analysis revealed no significant trends in α over time ($p = 0.07$, $R^2 = 0.22$ for K1; $p = 0.21$, $R^2 = 0.11$ for O1). (b) Yearly attenuation coefficients (β) for O1 and K1. Linear regression analysis showed significant decreasing trends in β ($p < 0.001$, $R^2 = 0.71$ for K1; $p < 0.001$, $R^2 = 0.81$ for O1). Error bars and shaded areas in (a) and (b) represent 95 % confidence intervals based on error propagation. (c) Predicted ratios for O1(solid line) and K1 (dotted line) versus distance from the coastline.

agreement with observed reductions in land area above MSL, especially between 1975 and 2014. Nevertheless, even with the halved rate, projections still overestimate historical land area above MSL, particularly for the period before 1975 (Fig. 8a). These findings align with numerous studies of coastal wetlands (Blum and Roberts, 2009; Day et al., 2000), showing that sedimentation can significantly offset subsidence Specifically, our results indicate that this effect may have been most significant between 1975 and 2014, with potentially higher sedimentation rates before 1975. Moreover, sedimentation rates during these periods could have been influenced by shifts in sediment loads due to river management, changes in compaction rates, localized erosion patterns, and anthropogenic activities like oil and gas extraction since the early 1970s (Day et al., 2020; Edmonds et al., 2023; Kolker et al., 2011).

Fig. 8b shows the projected land areas from 1932 to 2014 using the halved land subsidence rate. Overall, the projections align well with observed land loss in the outer regions near the fastland in southern Barataria between 1956 and 1975, including areas adjacent to Bayou Lafourche and south of Lake Salvador. This suggests that the overall land subsidence rate likely has decreased in recent two decades. However, in some coastal areas, the projections indicate more land area than observed in historical data (compare Fig. 8b with Fig. 1b). For instance, our projections depict the southeastern Barataria Basin as predominantly land in 1932, whereas historical observations show scattered water bodies. These differences may result from factors not fully accounted for in our analysis, such as sedimentation processes, potential inaccuracies in the Digital Elevation Model (DEM) at low elevations, uncertainties in historical marshland measurements, and temporal and/or spatial variations in land subsidence rate. Despite these discrepancies, our study provides a baseline for understanding land area changes over time in the Barataria Basin. Although numerous studies have examined historical land loss in coastal Louisiana, our approach—combining land subsidence, sea-level rise, and changing tidal amplitudes—offers a fresh perspective on how these processes collectively shape this interdistributary basin. Despite certain uncertainties, the results provide a reference point for understanding their combined effects on land area changes.

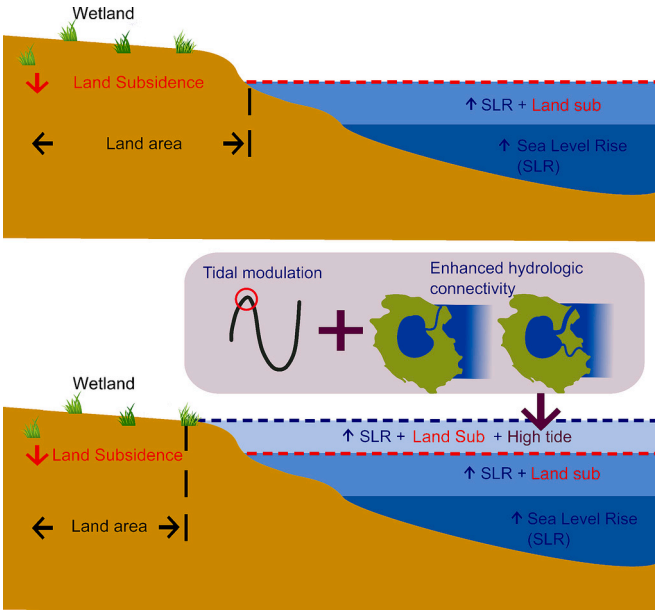

Fig. 7. Conceptual diagram illustrating how high tides, resulting from tidal modulation and enhanced hydrological connectivity, expand the spatial extent of nuisance flooding.

4.3. Land area comparison

Following the analysis of historical land area changes, we examined how the extent of emergent land area changes under different water level scenarios. Fig. 9 compares imagery at different water levels, showing that the Bayou des Allemands area, largely exposed at a MSL, is significantly inundated at a higher water level. This indicates the area's sensitivity to water level changes and suggests potential vulnerability to future sea-level rise and increased tidal influence.

Tides propagate inland at different rates, so high-water levels rarely peak simultaneously across the region; phase lags typically increase with distance from the coastline. For instance, Zumberge et al. (2022) documented diurnal water-level lags of several hours among CRMS stations only a few tens of kilometers apart in mid-Barataria. Consequently, our MHHW-based land area predictions assume high tide everywhere at once. In reality, the emergent land at any single moment is likely larger than the MHHW-predicted area due to asynchronous tidal peaks.

4.4. Predicted land loss: Implications of tidal variations

We predicted the potential inundation of land area over time in the Barataria region, with a particular emphasis on the impact of MHHW. From 2017 to 2022, the difference between the predicted MSL land area and the MHHW land area is negligible (Fig. 10a and b). However, this discrepancy begins to widen considerably by 2045. For the year 2045, the land area potentially inundated by MHHW with a halved subsidence rate was approximately 65 % (~1090 km^2) of the land area above MSL

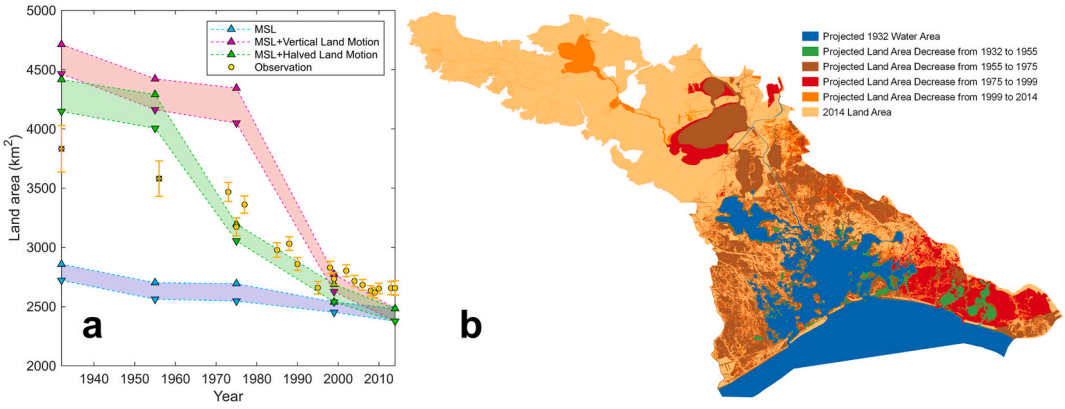

Fig. 8. Projected and observed historical land area changes in the Barataria Basin (1932–2014). (a) Comparison of projected and observed land area. Triangles and inverted triangles represent projections based on four-pixel and zero-pixel connectivity, respectively.
Observed land areas from surveys and aerial photos (1932 and 1955) are indicated by 'x' symbols, with Landsat measurements providing additional reference data (1975–2014; Couvillion et al. (2017)). Error bars represent ±1.96 standard errors, illustrating the uncertainty in the measurements. (b) Projected land area changes based on mean sea level (MSL) and a halved land subsidence rate.

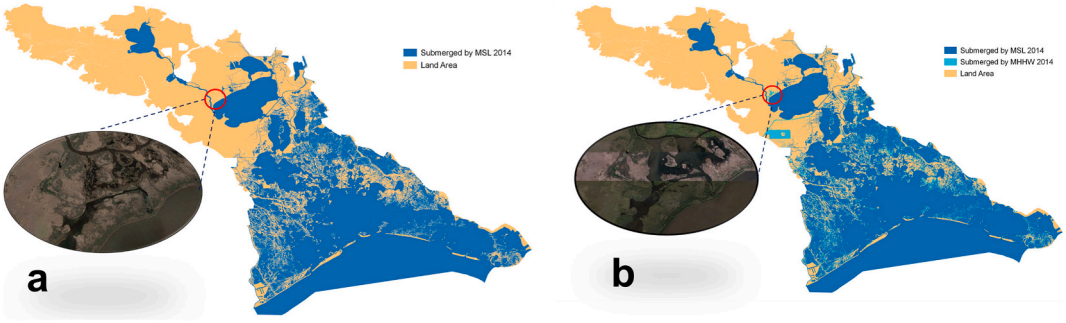

Fig. 9. Influence of water level variations on land-sea distribution in 2014–2015. Satellite images from January 2015 (a) and October 2014 (b) illustrate how land can transition between emergent and submerged states due to tidal and other water level variations.

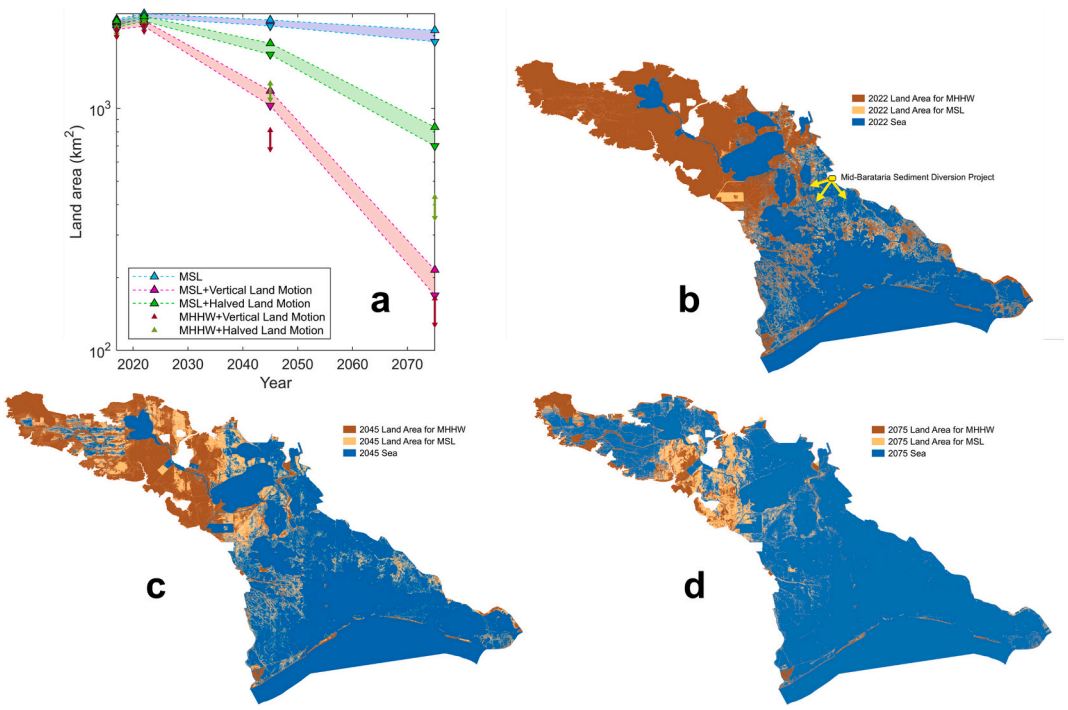

Fig. 10. Predicted land area changes in the Barataria Basin (2017–2075). (a) Predicted land area based on four-way (triangles) and zero-way (inverted triangles) connectivity. (b-d) Predicted land-sea distribution for 2022 (b), 2045 (c), and 2075 (d), assuming a halved land subsidence rate. The location of Mid-Barataria Sediment Diversion (MBSD) is also shown as a reference in panel (b).

with a halved subsidence rate (~1672 km^2). This estimation was similar to the land area estimated MSL assuming full subsidence rate (~1027 km^2).

The broadening gap between land area predictions based on MSL and those considering high-tide water levels highlights the growing risk of frequent and extensive high-tide inundation in low-lying areas of the Barataria Basin. For example, in the lower Barataria region, our prediction for 2045 (assuming a halved land subsidence rate) indicate that a considerable portion of fragmented marshland would remain above MSL (Fig. 10c). However, during high tides, much of this marsh area is predicted to be inundated, with the exception of some higher elevations on the barrier islands. Similarly, in the upper Barataria region, areas around Lac des Allemands, Lake Cataouatche, and south to Lake Salvador are predicted to experience frequent high-tide inundation by 2045, unlike the MSL-based prediction where much of this land remains similar to 2022. This trend indicates that by 2045, a substantial portion of the remaining land may have elevations close to MSL, making it increasingly vulnerable to prolonged high-tide inundation. More frequent and extended periods of high-tide inundation can intensify vegetation stress and hinder soil-building processes, potentially accelerating the transition to open water (Janousek and Mayo, 2013; Krask et al., 2022; Regine et al., 2018). Our model suggests that by 2075, only a small portion of land around Lake Salvador may remain above MSL, with most of the Barataria region potentially inundated during high tides (Fig. 10d).

These findings highlight the critical need for coastal restoration in the Barataria Basin (Fig. 10b). The MBSD designed to enhance marsh accretion with sediment-laden water, becomes increasingly important as tidal intrusion extends further inland (Allison and Meselhe, 2010; Törnqvist, 2023). Incorporating predictions of tidal propagation can help adapt sediment diversion operations to shifting water levels and hydrodynamics. Combining our data-driven models with specific MBSD operational scenarios could refine strategies for long-term coastal resilience (Day et al., 2007).

4.5. Limitations

While our analysis provides valuable insights into land loss and high-tide flooding potential, several limitations remain. Firstly, we did not explicitly model human interventions, including the planned MBSD, which is intended to increase sediment deposition and could influence future inundation patterns and potentially enhance accretion. The MBSD may reduce some predicted losses, so excluding it might overestimate future land loss in diversion-targeted areas, while newly deposited sediments could exhibit different compaction behaviors than older Holocene strata and introduce uncertainties in localized subsidence (Törnqvist et al., 2008). Secondly, our assumption of a constant land subsidence rate, does not capture the known temporal variability of subsidence, which could influence the accuracy of longer-term predictions. As demonstrated by a simple sensitivity test (Table A1), varying subsidence rates can significantly change future land-area predictions. Thirdly, our model does not fully represent the complex and evolving sedimentation and accretion processes in the Barataria Basin, which are important for maintaining wetland elevation relative to rising water levels. As highlighted by Edmonds et al. (2023), incorporating spatially variable subsidence, sediment transport, and marsh accretion models is crucial for improving predictive accuracy.

Despite its limitations, our analysis builds on prior research by highlighting how land subsidence and evolving tidal dynamics jointly drive land loss and flood risk in a tidal-influenced interdistributary basin. This integrated perspective complements existing studies in coastal Louisiana and may guide similar assessments worldwide.

5. Conclusions

This study highlights the increasing potential for inundation in the Barataria Basin due to the combined effects of land subsidence, sea-level rise, and increasing tides. Our analysis highlights the growing influence of tidal intrusion in increasing the extent and frequency of future inundation. For the Barataria Basin, land subsidence and sea-level rise appear to reduce the attenuation of tidal propagation, amplifying the

range of inland water heights and increasing the potentially inundated area during high tides. Effective strategies for mitigating the impacts of increased inundation require careful consideration of these interacting factors, along with a comprehensive understanding of wetland accretion processes and ecological responses to changing hydrological conditions.

CRediT authorship contribution statement

Byungho Kang: Writing – original draft, Visualization, Software, Methodology, Investigation, Formal analysis, Data curation, Conceptualization. **Surui Xie:** Writing – review & editing, Validation, Supervision, Resources, Project administration, Methodology, Investigation, Funding acquisition, Conceptualization.

Declaration of competing interest

The authors declare that they have no known competing financial interests or personal relationships that could have appeared to influence the work reported in this paper.

Acknowledgments

This research was supported by start-up funds from University of Houston. The work was also supported by the Korea Institute of Energy Technology Evaluation and Planning (KETEP) and the Ministry of Trade, Industry & Energy (MOTIE) of the Republic of Korea (No. 20223030020130, "Development of Design Technology for TLP-type Floating Offshore Wind Turbine System and Scaled Model Test Technique") and the Framework of the Research and Development Program of the Korea Institute of Energy Research (KIER) [grant number C5-2418]. The authors express their gratitude to Dr. Torbjörn E. Törnqvist at Tulane University for providing the source for vertical motion data integral to this study. We also acknowledge Brady Couvillion from the United States Geological Survey (USGS) for contributing the geographical data for fastland, which delineated the scope of our analysis and offered valuable insights into the region.

Appendix A. Supplementary data

Supplementary data to this article can be found online at https://doi.org/10.1016/j.seares.2025.102594.

Data availability statement

The topobathymetric digital elevation model (TBDEM) utilized in this research is accessible through the USGS EarthExplorer database (https://earthexplorer.usgs.gov/). Vertical land motion data, obtained via Rod Surface Elevation Tables (RSET), are available in Supplementary Data 1 of the publication "Vulnerability of Louisiana's Coastal Wetlands to Present-Day Rates of Relative Sea-Level Rise" (https://www.nature.com/articles/ncomms14792). Quality-assured water elevation measurements, collected from Coastal Restoration Monitoring System (CRMS) tidal gauges, can be accessed via the CRMS network (https://cims.coastal.louisiana.gov/monitoring-data/).

References

Allison, M.A., Meselhe, E.A., 2010. The use of large water and sediment diversions in the lower Mississippi River (Louisiana) for coastal restoration. J. Hydrol. 387 (3–4), 346–360.

Allison, M.A., Ramirez, M.T., Meselhe, E.A., 2014. Diversion of Mississippi River water downstream of New Orleans, Louisiana, USA to maximize sediment capture and ameliorate coastal land loss. Water Resour. Manag. 28 (12), 4113–4126. https://doi.org/10.1007/s11269-014-0731-y.

Anderson, T.R., Fletcher, C.H., Barbee, M.M., Romine, B.M., Lemmo, S., Delevaux, J.M. S., 2018. Modeling multiple sea level rise stresses reveals up to twice the land at risk compared to strictly passive flooding methods. Sci. Rep. 8 (1), 14484. https://doi.org/10.1038/s41598-018-32658-x. , Sep 27.

Blum, M.D., Roberts, H.H., 2009. Drowning of the Mississippi Delta due to insufficient sediment supply and global sea-level rise. Nat. Geosci. 2 (7), 488–491. https://doi.org/10.1038/ngeo553.

Bowman, P., Perret, W., Roussel, J., 1995. Freshwater Introduction and Implications for Fisheries Production in Louisiana.

Brown, S., Nicholls, R.J., 2015. Subsidence and human influences in mega deltas: the case of the Ganges–Brahmaputra–Meghna. Sci. Total Environ. 527-528, 362–374. https://doi.org/10.1016/j.scitotenv.2015.04.124.

Byrnes, M.R., Britsch, L.D., Berlinghoff, J.L., Johnson, R., Khalil, S., 2019. Recent subsidence rates for Barataria Basin, Louisiana. Geo-Mar. Lett. 39 (4), 265–278. https://doi.org/10.1007/s00367-019-00573-3.

Cheng, F.Y., Van Meter, K.J., Byrnes, D.K., Basu, N.B., 2020. Maximizing US nitrate removal through wetland protection and restoration. Nature 588 (7839), 625–630. https://doi.org/10.1038/s41586-020-03042-5.

Costanza, R., de Groot, R., Sutton, P., van der Ploeg, S., Anderson, S.J., Kubiszewski, I., Farber, S., Turner, R.K., 2014. Changes in the global value of ecosystem services. Glob. Environ. Chang. 26, 152–158. https://doi.org/10.1016/j.gloenvcha.2014.04.002.

Couvillion, B.R., Fischer, M.R., Beck, H.J., Sleavin, W.J., 2016. Spatial configuration trends in coastal Louisiana from 1985 to 2010. Wetlands 36 (2), 347–359. https://doi.org/10.1007/s13157-016-0744-9.

Couvillion, B.R., Beck, H., Schoolmaster, D., Fischer, M., 2017. Land area change in coastal Louisiana (1932 to 2016) [Report](3381). (Scientific Investigations Map, Issue. U. S. G. Survey). http://pubs.er.usgs.gov/publication/sim3381.

CPRA, 2018. Mid-Barataria and Mid-Breton Sediment Diversions: Overview & Frequently Asked Questions. https://coastal.la.gov/wp-content/uploads/2018/03/OVERVIEW_FAQs_Mid-Barataria-and-Mid-Breton-Sediment-Diversions.pdf.

CPRA, 2022. Coastal Information Management System (CIMS) Data Dictionary. https://cims.coastal.louisiana.gov/RecordDetail.aspx?Root=0&sid=11505.

Das, A., Justic, D., Inoue, M., Hoda, A., Huang, H., Park, D., 2012. Impacts of Mississippi River diversions on salinity gradients in a deltaic Louisiana estuary: ecological and management implications. Estuar. Coast. Shelf Sci. 111, 17–26. https://doi.org/10.1016/j.ecss.2012.06.005.

Day, J.W., Martin, J.F., Cardoch, L., Templet, P.H., 1997. System functioning as a basis for sustainable management of deltaic ecosystems. Coast. Manag. 25 (2), 115–153. https://doi.org/10.1080/08920759709362315.

Day, J.W., Britsch, L.D., Hawes, S.R., Shaffer, G.P., Reed, D.J., Cahoon, D., 2000. Pattern and process of land loss in the Mississippi Delta: a spatial and temporal analysis of wetland habitat change. Estuaries 23 (4), 425–438. https://doi.org/10.2307/1353136.

Day, J.W., Boesch, D.F., Clairain, E.J., Kemp, G.P., Laska, S.B., Mitsch, W.J., Orth, K., Mashriqui, H., Reed, D.J., Shabman, L., Simenstad, C.A., Streever, B.J., Twilley, R.R., Watson, C.C., Wells, J.T., Whigham, D.F., 2007. Restoration of the Mississippi Delta: lessons from hurricanes Katrina and Rita. Science 315 (5819), 1679–1684. https://doi.org/10.1126/science.1137030.

Day, J.W., Clark, H.C., Chang, C., Hunter, R., Norman, C.R., 2020. Life cycle of oil and gas fields in the Mississippi River Delta: a review. Water 12 (5), 1492. https://www.mdpi.com/2073-4441/12/5/1492.

Didier, D., Baudry, J., Bernatchez, P., Dumont, D., Sadegh, M., Bismuth, E., Bandet, M., Dugas, S., Sévigny, C., 2019. Multihazard simulation for coastal flood mapping: bathtub versus numerical modelling in an open estuary, eastern Canada. J. Flood Risk Manag. 12 (S1), e12505. https://doi.org/10.1111/jfr3.12505.

Edmonds, D.A., Toby, S.C., Siverd, C.G., Twilley, R., Bentley, S.J., Hagen, S., Xu, K., 2023. Land loss due to human-altered sediment budget in the Mississippi River Delta. Nat. Sustain. https://doi.org/10.1038/s41893-023-01081-0.

Feng, X., Feng, H., 2021. On the role of anthropogenic activity and sea-level-rise in tidal distortion on the open coast of the Yellow Sea shelf. J. Geophys. Res. Oceans 126 (3). https://doi.org/10.1029/2020JC016583 e2020JC016583.

Gagliano, S.M., Meyerarendt, K.J., Wicker, K.M., 1981. Land loss in Mississippi River deltaic plain. AAPG Bull. 65 (9), 1684–1685. https://archives.datapages.com/data/bulletns/1980-81/data/pg/0065/0009/1650/1684c.htm.

Gallien, T.W., Schubert, J.E., Sanders, B.F., 2011. Predicting tidal flooding of urbanized embayments: a modeling framework and data requirements. Coast. Eng. 58 (6), 567–577. https://doi.org/10.1016/j.coastaleng.2011.01.011.

García, M., Saatchi, S., Ustin, S., Balzter, H., 2018. Modelling forest canopy height by integrating airborne LiDAR samples with satellite radar and multispectral imagery. Int. J. Appl. Earth Obs. Geoinf. 66, 159–173. https://doi.org/10.1016/j.jag.2017.11.017.

Gornitz, V., White, T.W., Cushman, R.M., 1991. *Vulnerability of the US to future sea level rise* Conference: 7. symposium on coastal and ocean management, Long Beach, CA (USA), 8-12 Jul 1991, United States. https://www.osti.gov/biblio/5875484.

Holzer, T.L., Bluntzer, R.L., 1984. Land subsidence near oil and gas fields, Houston, Texasa. Groundwater 22 (4), 450–459. https://doi.org/10.1111/j.1745-6584.1984.tb01416.x.

Hsiao, S.-C., Fu, H.-S., Wu, H.-L., Liang, T.-Y., Chang, C.-H., Chen, Y.-M., Lin, L.-Y., Chen, W.-B., 2024. Impact assessment of sea level rise-induced high tide flooding and socioeconomic losses in a highly vulnerable coastal region. J. Hydrol. Reg. Stud. 55, 101921. https://doi.org/10.1016/j.ejrh.2024.101921.

Inoue, M., Park, D., Justic, D., Wiseman, W.J., 2008. A high-resolution integrated hydrology–hydrodynamic model of the Barataria Basin system. Environ. Model Softw. 23 (9), 1122–1132. https://doi.org/10.1016/j.envsoft.2008.02.011.

Jankowski, K.L., Tornqvist, T.E., Fernandes, A.M., 2017. Vulnerability of Louisiana's coastal wetlands to present-day rates of relative sea-level rise. Nat. Commun. 8, 14792. https://doi.org/10.1038/ncomms14792.

Janousek, C. N., & Mayo, C. (2013, 2013/07/01). Plant responses to increased inundation and salt exposure: interactive effects on tidal marsh productivity. Plant Ecol., 214(7), 917–928. doi:https://doi.org/10.1007/s11258-013-0218-6.

Kang, B., Xie, S., 2024. Enhanced tidal intrusion in the Barataria Basin, Mississippi River Delta. J. Coast. Res. 41 (2), 336–346. https://doi.org/10.2112/JCOASTRES-D-24-00047.1.

Karegar, M.A., Dixon, T.H., Malservisi, R., 2015. A three-dimensional surface velocity field for the Mississippi Delta: implications for coastal restoration and flood potential. Geology 43 (6), 519–522. https://doi.org/10.1130/g36598.1.

Karegar, M.A., Larson, K.M., Kusche, J., Dixon, T.H., 2020. Novel quantification of shallow sediment compaction by GPS interferometric reflectometry and implications for flood susceptibility. Geophys. Res. Lett. 47 (14). https://doi.org/10.1029/2020GL087807 e2020GL087807.

Kolker, A.S., Allison, M.A., Hameed, S., 2011. An evaluation of subsidence rates and sea-level variability in the northern Gulf of Mexico. Geophys. Res. Lett. 38 (21). https://doi.org/10.1029/2011GL049458.

Krask, J.L., Buck, T.L., Dunn, R.P., Smith, E.M., 2022. Increasing tidal inundation corresponds to rising porewater nutrient concentrations in a southeastern U.S. salt marsh. PLoS One 17 (11), e0278215. https://doi.org/10.1371/journal.pone.0278215.

Matsushita, T., Ghezelloo, Y., Maly, E., Kondo, T., Meyer, M., Newman, G., 2024. Placemaking mediating dilemmas by addressing the gaps in post-disaster recovery process: long-term citizen-driven place-nurturing in New Orleans after hurricane Katrina. Int. J. Disaster Risk Reduction 106, 104457. https://doi.org/10.1016/j.ijdrr.2024.104457.

Mostafiz, R.B., Bushra, N., Rohli, R.V., Friedland, C.J., Rahim, M.A., 2021. Present vs. future property losses from a 100-year coastal flood: a case study of grand isle, Louisiana. Front. Water 3. https://doi.org/10.3389/frwa.2021.763358.

Nelson, S.A.C., Soranno, P.A., Qi, J., 2002. Land-cover change in upper Barataria Basin estuary, Louisiana, 1972–1992: increases in wetland area. Environ. Manag. 29 (5), 716–727. https://doi.org/10.1007/s00267-001-0060-9.

Nienhuis, J.H., Törnqvist, T.E., Jankowski, K.L., Fernandes, A.M., Keogh, M.E., 2017. A new subsidence map for coastal Louisiana. GSA Today 27 (9), 2. https://doi.org/10.1130/GSATG337GW.1.

Pahl, J., 2017. Coastal Master Plan: Attachment C-2: eustatic sea Level Rise (Coastal Protection and Restoration Authority: Baton Rouge, LA, USA, Issue). https://coastal.la.gov/wp-content/uploads/2017/04/Attachment-C2-1_FINAL_3.16.2017.pdf.

Pawlowicz, R., Beardsley, B., Lentz, S., 2002. Classical tidal harmonic analysis including error estimates in MATLAB using T_TIDE. Comput. Geosci. 28 (8), 929–937. https://doi.org/10.1016/S0098-3004(02)00013-4.

Poulter, B., Halpin, P.N., 2008. Raster modelling of coastal flooding from sea-level rise. Int. J. Geogr. Inf. Sci. 22 (2), 167–182. https://doi.org/10.1080/13658810701371858.

Regine, R., Thomas, D., Dietrich, H., Christoph, L., 2018. Effects of inundation, nutrient availability and plant species diversity on fine root mass and morphology across a saltmarsh flooding gradient. Front. Plant Sci. 9. https://doi.org/10.3389/fpls.2018.00098.

Roberts, H.H., 1997. Dynamic changes of the Holocene Mississippi River Delta plain: the Delta cycle. J. Coast. Res. 13 (3), 605–627. http://www.jstor.org/stable/4298659.

Seenath, A., Wilson, M., Miller, K., 2016. Hydrodynamic versus GIS modelling for coastal flood vulnerability assessment: which is better for guiding coastal management? Ocean Coast. Manag. 120, 99–109. https://doi.org/10.1016/j.ocecoaman.2015.11.019.

Shirzaei, M., Freymueller, J., Törnqvist, T.E., Galloway, D.L., Dura, T., Minderhoud, P.S. J., 2021. Measuring, modelling and projecting coastal land subsidence. Nat. Rev Earth Environ. 2 (1), 40–58. https://doi.org/10.1038/s43017-020-00115-x.

Sweet, W., Dusek, G., Obeysekera, J.T.B., Marra, J.J., 2018. Patterns and projections of high tide flooding along the U.S. coastline using a common impact threshold [Technical Report]. https://doi.org/10.7289/V5/TR-NOS-COOPS-086 (NOAA technical report NOS CO-OPS; 086).

Thompson, P.R., Widlansky, M.J., Hamlington, B.D., Merrifield, M.A., Marra, J.J., Mitchum, G.T., Sweet, W., 2021. Rapid increases and extreme months in projections of United States high-tide flooding. Nat. Clim. Chang. 11 (7), 584–590. https://doi.org/10.1038/s41558-021-01077-8.

Törnqvist, T.E., 2023. A river delta in transition. Nat. Sustain. 6 (6), 617–618. https://doi.org/10.1038/s41893-023-01104-w.

Törnqvist, T.E., Wallace, D.J., Storms, J.E.A., Wallinga, J., van Dam, R.L., Blaauw, M., Derksen, M.S., Klerks, C.J.W., Meijneken, C., Snijders, E.M.A., 2008. Mississippi Delta subsidence primarily caused by compaction of Holocene strata. Nat. Geosci. 1 (3), 173–176. https://doi.org/10.1038/ngeo129.

USACE, 2022. Environmental Impact Statement For The Propose Mid-Barataria Sediment Diversion Project [Government Report]. https://usace.contentdm.oclc.org/digital/collection/p16021coll9/id/2978.

USGS, 2018. USGS EROS Archive - Digital Elevation - Coastal National Elevation Database (CoNED) Project - Topobathymetric Digital Elevation Model (TBDEM) [gif]. https://doi.org/10.5066/F7Z60MHJ.

Vaccare, J., Meselhe, E., White, J.R., 2019. The denitrification potential of eroding wetlands in Barataria Bay, LA, USA: implications for river reconnection. Sci. Total Environ. 686, 529–537. https://doi.org/10.1016/j.scitotenv.2019.05.475.

Yang, Z., Wang, T., Leung, R., Hibbard, K., Janetos, T., Kraucunas, I., Rice, J., Preston, B., Wilbanks, T., 2014. A modeling study of coastal inundation induced by storm surge, sea-level rise, and subsidence in the Gulf of Mexico. Nat. Hazards 71 (3), 1771–1794. https://doi.org/10.1007/s11069-013-0974-6.

Yunus, A., Avtar, R., Kraines, S., Yamamuro, M., Lindberg, F., Grimmond, C., 2016. Uncertainties in tidally adjusted estimates of sea level rise flooding (bathtub model) for the greater London. Remote Sens. 8 (5). https://doi.org/10.3390/rs8050366.

Zumberge, M.A., Xie, S., Wyatt, F.K., Steckler, M.S., Li, G., Hatfield, W., Elliott, D., Dixon, T.H., Bridgeman, J.G., Chamberlain, E.L., Allison, M., Törnqvist, T.E., 2022. Novel integration of geodetic and geologic methods for high-resolution monitoring of subsidence in the Mississippi Delta. J. Geophys. Res. Earth 127 (9). https://doi.org/10.1029/2022JF006718 e2022JF006718.